Journal of Materials Chemistry C

RSC Publishing

PAPER

View Article Online
View Journal | View Issue

Cite this: J. Mater. Chem. C, 2013, 1, 4962

3-Hydroxycinnamic acid – a new central core for the design of bent-shaped liquid crystals†

Michal Kohout,[a] Jiří Tůma,[a] Jiří Svoboda,[a] Vladimíra Novotná,*[b] Ewa Gorecka[c] and Damian Pociecha[c]

Received 10th April 2013
Accepted 11th June 2013

DOI: 10.1039/c3tc30664j

www.rsc.org/MaterialsC

The synthesis and mesomorphic properties of a new series of bent-shaped liquid crystals based on 3-hydroxycinnamic acid are presented. Prepared compounds differ in the orientation of an ester linking group in one of the side arms. Additionally, the mesomorphic properties have been tuned by employing either an alkoxy or carboxylic terminal group and by varying the length of terminal alkyl chains. Texture observation and calorimetric studies, as well as electro-optics, X-ray and dielectric measurements have been performed. Influence of the ester linking group orientation and the length of the terminal alkyl chain on mesomorphic behaviour has been established. Out of 12 studied compounds only one formed lamellar phases, namely the B_2–B_5 phase sequence, while all other exhibited columnar phases, either B_1 or B_{1Rev} type, depending on the direction of the ester group. Structural properties of the columnar phases have been studied in detail using X-ray diffraction techniques for pure materials as well as for binary mixtures of compounds forming the B_1 and B_{1Rev} phase. All results are discussed with respect to the molecular structure.

1 Introduction

Bent-shaped mesogens have become an integral part of liquid crystal research in the past few years. Since the discovery of polar chiral phases and ferroelectric switching from achiral bent-shaped mesogens[1] detailed studies on the structure–property relationships have been published and summarized in various reviews.[2,3] Recently, functionalized bent-shaped materials feasible for electro-optical applications have also been developed.[4,5] This required designing liquid crystalline compounds, which possess additional functional groups (*e.g.* a double bond) in their molecular structure. The double bond of cinnamic acid has already been of interest in the field of liquid crystals[6–8] as it enables modification of their mesomorphic behaviour by illumination. This approach was utilized to double bond isomerisation and thus to switching the mesomorphic properties,[7] and to photodimerisation and cross-linking the molecules in the liquid crystalline state.[8] The cinnamate structural motif was also occasionally applied in the design of bent-shaped mesogens.[5,9,10] Most of the studied compounds possessed the cinnamate connecting unit in the outer position of the lengthening arms.[9] On the other hand, an example of a material with the cinnamate unit joined to the central core[5] and some series of compounds with a reversed orientation of the cinnamate unit in the outer position[11] have been reported. Their mesomorphic properties have also been modified by the lateral substitution of a cinnamate double bond by methyl[9,10] and cyano[5] groups. The role of ester linking groups has been established for bent-shaped compounds with benzene[12] and naphthalene[13] central units and it has been found that the ester orientation strongly influences the mesomorphic properties.

The most studied mesophase of bent-shaped materials is a lamellar B_2 phase, in which molecules are closely packed in layers and tilted with respect to the layer normal. For the B_2 phase the notation SmCP has been often utilized with the index S or A at the letter C, which describes the synclinic or anticlinic orientation of the tilt in neighbouring layers, respectively. Letter P stands for a polarization state and the corresponding subscript index F or A expresses ferroelectricity or antiferroelectricity of the lamellar system,[3] respectively. The antiferroelectric type of switching is preferably observed in the B_2 phases. Additionally, another switchable smectic phase with tilted molecules has been found and, according to the nomenclature, designated B_5. The B_5 phase exhibits a long range order (2D lattice) within the layers, but no positional correlations between layers.[2,14] Until now only a few examples of the B_5 phase have been presented and properly characterized by X-ray diffraction.

[a]Department of Organic Chemistry, Institute of Chemical Technology, CZ-166 28 Prague 6, Czech Republic. E-mail: Jiri.Svoboda@vscht.cz; Fax: +420 220444182; Tel: +420 220444288

[b]Institute of Physics, Academy of Science of the Czech Republic, Na Slovance 2, CZ-182 21 Prague 9, Czech Republic. E-mail: novotna@fzu.cz; Fax: +420 286890527; Tel: +420 266053111

[c]Laboratory of Dielectrics and Magnetics, Chemistry Department, Warsaw University, Al. Zwirki i Wigury 101, 02-089 Warsaw, Poland. E-mail: pociu@chem.uw.edu.pl; Fax: +48 228221075; Tel: +48 228221075

† Electronic supplementary information (ESI) available. See DOI: 10.1039/c3tc30664j

Several columnar mesophases were found for the bent-shaped mesogens that are built from the layer fragments (molecular blocks) arranged in a two dimensional (2D) lattice. First, the columnar B_1 phase has been described with a density modulation in the plane parallel to the polarization vector, ***P***. In the B_1 phase no electro-optic response and switching current were observed. When the density modulation plane is perpendicular to the ***P*** vector, the nomenclature of the B_{1Rev} phase was proposed.[15] These phases can switch under the electric field and exist in different variants: with tilted or non-tilted molecules with respect to the layer fragment normal.

In this paper we report on synthesis and mesomorphic properties of new bent-shaped materials based on a 3-hydroxycinnamic acid central core. Such a molecular core is utilized in the design of the bent-shaped mesogens for the first time. With respect to analogous compounds based on the naphthalene core,[13] in this new non-symmetrical central unit one of the fused benzene rings is reduced to a single double bond. As a consequence of a lower rigidity and a change of the packing mode one can expect lower transition temperatures and different mesomorphic properties in comparison with naphthalene-core bent-shaped compounds. Three series of new materials were synthesised differing in the number and orientation of ester groups in the lengthening arms. The properties of new compounds were investigated by differential scanning calorimetry (DSC), polarizing optical microscopy and selected samples were studied by X-ray diffraction and dielectric measurements. Structural parameters of different columnar phases were analysed and compared. Binary mixtures of homologues with reversed orientation of the ester group revealing different types of the columnar phase were prepared and their parameters were studied.

2 Experimental

The synthetic pathway for the target compounds **I–III** is shown in Scheme 1. First, the hydroxylic group of the starting 3-hydroxycinnamic acid was protected with the *tert*-butyl-(dimethyl)silyl group (TBDMS) to yield the protected acid **1**. In the next step, the first lengthening arm was introduced in a *N*,*N*′-dicyclohexylcarbodiimide (DCC) mediated esterification of acid **1** with the corresponding hydroxy esters **2A–L** in the presence of *N*,*N*-dimethylaminopyridine (DMAP) as a catalyst. Subsequently, the protecting silyl group in the formed intermediate **3** was removed by means of tetrabutylammonium fluoride (TBAF) in wet tetrahydrofuran (THF) and the released hydroxylic group in esters **4** was finally acylated by acid chlorides **5A–D** of the second lengthening arm, giving rise to the target compounds **I–III** (Scheme 1).

Syntheses of the lengthening arms of the target materials, 4-alkoxyphenyl 4-hydroxybenzoates (**2A–D**), 4-hydroxyphenyl 4-alkoxybenzoates (**2E–H**), alkyl 4-[(4-hydroxybenzoyl)oxy]-benzoates (**2I–L**) and 4-[(4-alkoxybenzoyl)oxy]benzoic acid chlorides (**5A–D**) (**A**, **E**, **I** with R = octyl, **B**, **F**, **J** with R = decyl, **C**, **G**, **K** with R = dodecyl, and **D**, **H**, **L** with R = tetradecyl), were described previously.[13a,16]

The sequence of phases and phase transition temperatures were determined from optical textures and their changes were observed under a polarizing optical microscope (Nikon Eclipse E600Pol). The Linkam LTS E350 heating/cooling stage with a TMS 93 temperature programmer was used for the temperature control, which enabled temperature stabilization within ±0.1 K. The planar samples for the texture observation and electro-optical studies were made from glasses with ITO transparent electrodes (5×5 mm^2), separated by mylar sheets defining the cell thickness. They were filled in the isotropic phase by capillary action. Free-standing films were prepared by spreading a compound in a liquid crystalline phase across a hole in the metallic plate.

For all compounds differential scanning calorimetry (DSC) was carried out by employing a Perkin-Elmer Pyris Diamond calorimeter. The samples of about 2–5 mg, hermetically sealed in aluminium pans, were placed in a nitrogen atmosphere in the calorimeter working place. The calorimeter data were calibrated on extrapolated onset temperatures and enthalpy changes of water, indium and zinc. The measurements were performed on cooling/heating runs at a rate of 5 K min^{-1}.

The switching properties were studied with driving voltage from a Phillips generator PM 5191, which is accompanied by a linear amplifier, providing the maximum amplitude of 120 V. The switching current profiles *vs.* time were recorded using a Tektronix memory oscilloscope DPO4034. Dielectric properties were studied using a Schlumberger 1260 impedance analyser. The frequency dispersions were measured in the range of 10 Hz to 10 MHz at a stabilized temperature during the cooling process at a rate of about 0.2 K min^{-1}. The dispersion data were analyzed using the Cole–Cole formula (1) in a generalized form. For the frequency dependent complex permittivity $\varepsilon^*(f) = \varepsilon' - i\varepsilon''$ we have utilized:

$$\varepsilon^* - \varepsilon_\infty = \frac{\Delta\varepsilon}{1 + (if/f_r)^{(1-\alpha)}} - i\left(\frac{\sigma}{2\pi\varepsilon_0 f^n} + Af^m\right), \qquad (1)$$

where f_r is the relaxation frequency, $\Delta\varepsilon$ is the dielectric strength, α is the distribution parameter of the relaxation, ε_0 is the permittivity of vacuum, ε_∞ is the high frequency permittivity and n, m, A are the parameters of fitting. The second and the third terms of the equation (in brackets) are used to eliminate a low frequency contribution from d.c. conductivity σ and a high frequency contribution due to the resistance of the electrodes, respectively. The real, ε', and imaginary, ε'', parts of permittivity were simultaneously fitted to (1) and the temperature dependences or f_r and $\Delta\varepsilon$ were plotted and analyzed.

The X-ray diffraction (XRD) studies were performed using a Bruker Nanostar system (CuKα radiation, cross-coupled Goebel mirrors, three pin-hole collimation, Vantec 2000 area detector, MRI TCPU H heating stage) and a Bruker GADDS system (CuKα radiation, Goebel mirror, point collimator and Vantec 2000 area detector, homemade heating stage). In both systems the temperature stability was 0.1 K. Powder samples (for Nanostar) were prepared in thin-walled glass capillaries (1.5 mm diameter), and partially oriented samples for experiments in reflection were prepared as droplets on a heated surface.

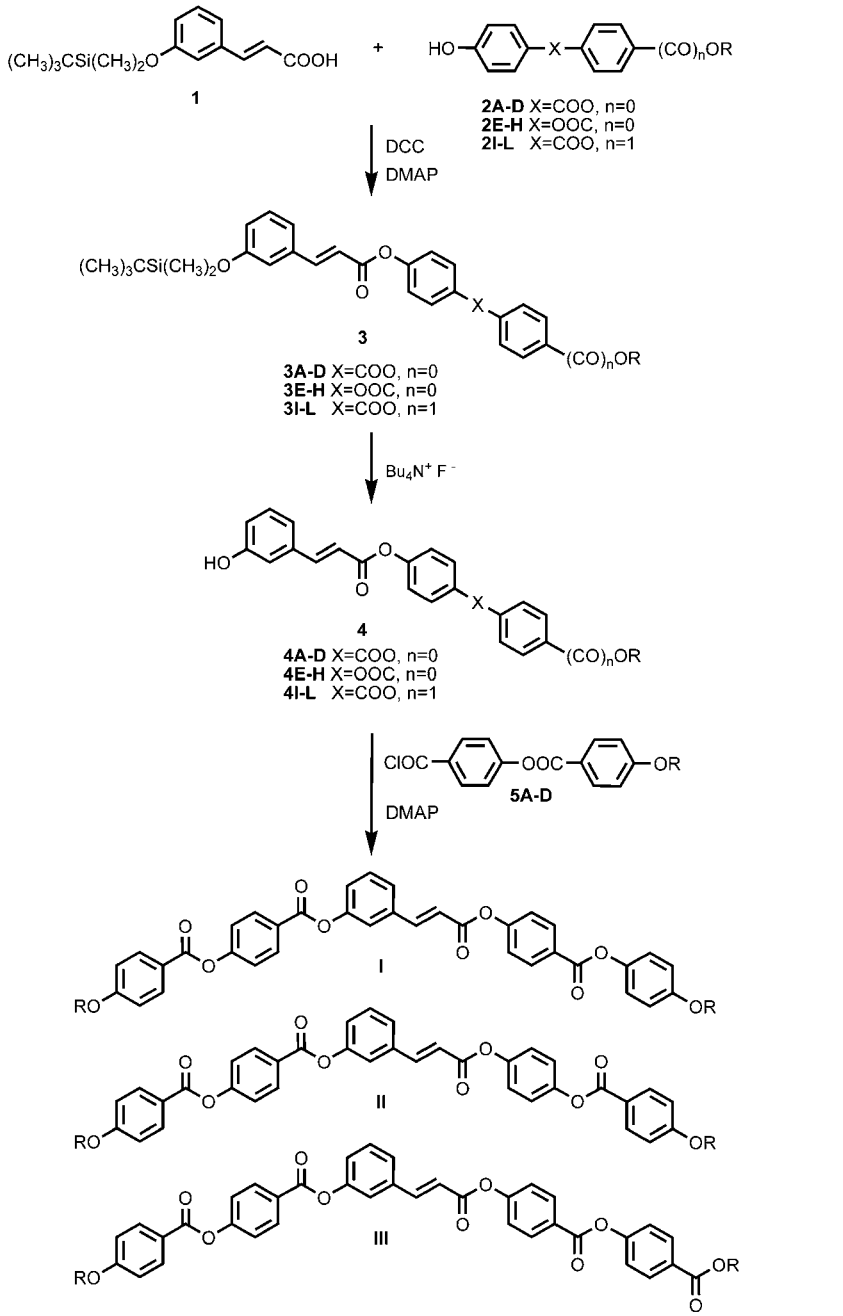

Scheme 1 The synthetic route and designation for compounds. Final compounds from series **I**, **II** and **III** were denoted with additional letters, **a** for R = C_8H_{17}, **b** for R = $C_{10}H_{21}$, **c** for R = $C_{12}H_{25}$ and **d** for R = $C_{14}H_{29}$.

3 Results

With respect to the number and orientation of the ester linking groups in the lengthening arms the materials are divided into three series denoted **I, II** and **III**. The left arm of compounds is identical and possesses two uniformly oriented ester units. Series **I** and **II** possess two ester groups in the right arm and differ in their orientation. Series **III** resembles series **I** concerning the ester orientation in the right arm, to which an additional ester group has been attached in the identical orientation, so there are five ester functionalities in total (see Scheme 1). DSC studies were performed for all compounds; the phase transition temperatures and associated enthalpy changes are summarized in Table 1. The DSC thermograms are shown in Fig. 1a–c for materials **Ib**, **IIb** and **IId**, respectively. For all studied materials, at least one enantiotropic mesophase has been observed. Phases and phase sequences have been identified by texture observation under the polarizing optical

Table 1 Phase transition temperatures, T_{tr}, in °C and the corresponding enthalpies, ΔH, were detected on the second cooling, melting points, M.p., on the second heating. All changes were performed at a rate of 5 K min^{-1}. The enthalpies are presented in brackets in kJ mol^{-1}. The position of the alkyl chain R is shown in Scheme 1

	R	M.p. (ΔH)	T_{cr} (ΔH)	M_2	T_{tr} (ΔH)	M_1	T_{tr} (ΔH)	Iso
Ia	C_8H_{17}	122 (+32.8)	105 (−27.5)			B_{1Rev}	159 (−21.3)	•
Ib	$C_{10}H_{21}$	121 (+29.0)	94 (−24.1)			B_{1Rev}	159 (−24.1)	•
Ic	$C_{12}H_{25}$	134 (+47.3)	97 (−26.3)			B_{1Rev}	158 (−22.3)	•
Id	$C_{14}H_{29}$	117 (+38.0)	100 (−31.0)			B_{1Rev}	157 (−22.7)	•
IIa	C_8H_{17}	87 (+32.9)	67 (−20.0)			B_1	147 (−21.8)	•
IIb	$C_{10}H_{21}$	101 (+30.7)	76 (−23.5)			B_1	139 (−23.8)	•
IIc	$C_{12}H_{25}$	92 (+18.5)	83 (−18.8)			B_1	135 (−21.0)	•
IId	$C_{14}H_{29}$	93 (+23.7)	76 (−25.9)	B_5	100 (−0.6)	B_2	136 (−13.5)	•
IIIa	C_8H_{17}	108 (+42.4)	102 (−39.0)			B_{1Rev}	153 (−15.1)	•
IIIb	$C_{10}H_{21}$	102 (+27.5)	98 (−27.0)			B_{1Rev}	152 (−7.2)	•
IIIc	$C_{12}H_{25}$	106 (+33.2)	102 (−32.5)			B_{1Rev}	156 (−13.2)	•
IIId	$C_{14}H_{29}$	104 (+30.4)	93 (−29.8)			B_{1Rev}	152 (−10.1)	•

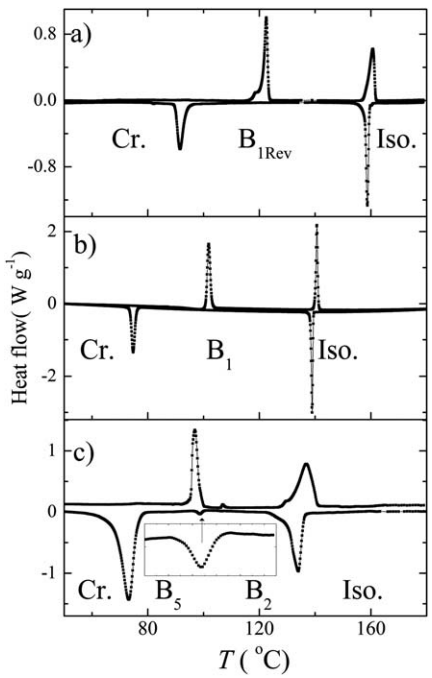

Fig. 1 Thermographs recorded for compounds (a) **Ib**, (b) **IIb** and (c) **IId** during the second heating and cooling runs (the upper and lower curves in each figure, resp.). Measurements were recorded at the rate of 5 K min^{-1}. The slopes are adjusted for convenience; mesophases are indicated. In the inset of (c) the B_2–B_5 phase transition (marked by an arrow in the cooling curve) is presented in an enlarged view.

microscope and confirmed by X-ray measurements (see the following paragraph). Switching properties and dielectric measurements have been studied as well.

We have also studied the intermediate silyl derivatives **3** and hydroxy derivatives **4** and found that **3E–H** and **4E–L** exhibited mesomorphic properties. Mesophases identification, phase transition temperatures and corresponding enthalpies are summarized in Table S1 in the ESI.† For silylated compounds **3E–H** a monotropic nematic phase was found. The homologue with the longest terminal chain **3H** exhibited polymorphism: the SmC phase was observed below the nematic phase. Enantiotropic nematic phases were identified for hydroxy derivatives **4E–J** and the SmA phase for compounds **4K–L** (see Table S1 in the ESI†).

For all compounds of the series **I** the columnar phase of B_{1Rev} type was identified regardless of the length of the terminal alkyl chain. Typical texture of the B_{1Rev} phase is shown in Fig. 2a for **Ia**. Under an applied electric field only the birefringence irreversibly changed, as shown in Fig. 2b. For the materials of series **II** with shorter terminal alkyl chains (C_8H_{17}–$C_{12}H_{25}$) the columnar B_1 phase has been identified. Typical mosaic textures of this phase are shown in Fig. 2c for compounds **IIa**. Materials of series **III** showed uniform mesomorphic behaviour and for all lengths of the terminal alkyl chain the columnar B_{1Rev} phase was found. Physical properties of the B_{1Rev} phase, observed in series **III**, are very similar to those of compounds **I**.

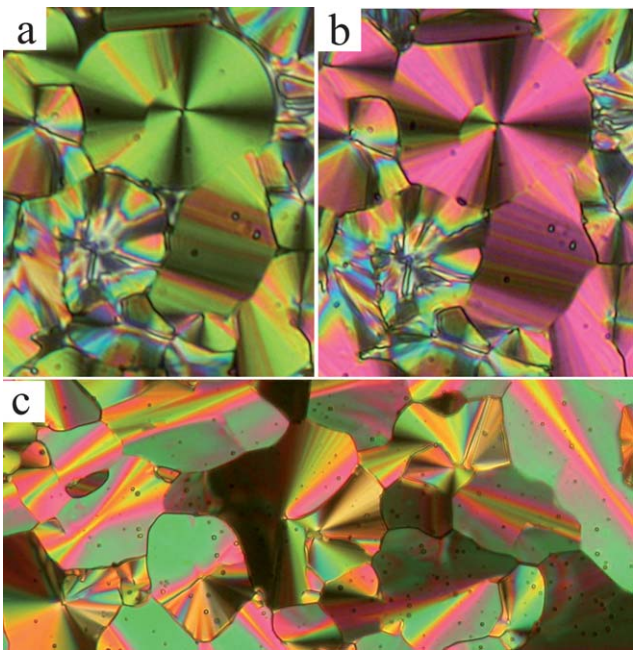

Fig. 2 Planar texture of compound **Ia** in the B_{1Rev} phase at 140 °C (a) before application of the electric field and (b) after switching off the field at about 50 V μm^{-1}. The width of each figure is 150 μm. (c) Mosaic texture of the B_1 phase for **IIa**. The width of the figure corresponds to 300 μm.

Two switchable phases have been observed for a homologue **IId** with the longest ($C_{14}H_{29}$) chain. For the higher temperature phase, which can be identified with a B_2 phase, the antiferroelectric character has been proved by the switching current profile (Fig. 3). From the planar textures and their behaviour (Fig. 4) under the applied electric field we can establish the character of the B_2 phase. Without electric field the overall extinction position is parallel to the smectic layer normal, which evidences anticlinicity (Fig. 4a). Under the weak electric field the birefringence slightly increases and at a threshold value of about 5 V μm^{-1} it abruptly grows up and the extinction brushes become inclined about 45 degrees from the layer normal within the whole sample (see Fig. 4b). The birefringence of the switched texture increases further with electric field up to the saturation at 10 V μm^{-1} (Fig. 4c). We consider that the ground state corresponds to the SmC_AP_A (antiferroelectric) phase and transforms to the SmC_SP_F (ferroelectric) phase under the applied electric field.

Another phase has been found below the B_2 phase on cooling for **IId**. Based on X-ray analysis, we attributed this phase to a B_5 phase with respect to the nomenclature. The structural character of the observed B_5 phase will be described later. The B_2–B_5 phase transition is accompanied by a small enthalpy change. Additionally, only a slight modification of textures has been observed in the planar (book-shelf) geometry as well as in the free-standing film. The antiferroelectric switching has been detected in the B_5 phase under an applied electric field, and the observed electro-optical response has been found comparable to that of the B_2 phase. We have measured the dielectric properties of compound **IId** in dependence on frequency and temperature within the temperature interval of the studied mesophases. One distinct mode has been observed in both mesophases and attributed to a collective dipolar character, as it completely disappears in the isotropic, as well as in the crystalline phases. The imaginary part of the permittivity, ε'', is presented *versus* frequency and temperature in Fig. 5. One can see a jump-like change of the mode strength at the B_2–B_5 phase transition. The temperature dependence of the fitting parameters for the dielectric spectroscopy data is presented in Fig. S2.† The relaxation frequency, f_r, decreases from 140 kHz, at the Iso–B_2 phase transition, to 40 kHz just before crystallization. A small jump-down change is detected on $f_r(T)$ at the B_2–B_5 phase transition. The dielectric strength is practically constant within the mesophase temperature range and can be evaluated as $\Delta\varepsilon = 4.5$ in the B_2 phase and $\Delta\varepsilon = 6$ in the B_5 phase. Temperature dependence of f_r in a logarithmic scale *versus* reciprocal temperature in Kelvins, $1/T$, is shown in Fig. 6. The linear dependence can be demonstrated in both mesophases with a clear change of the slope at the B_2–B_5 phase transition. It is evident that both dependences fulfil the Arrhenius law. We have calculated the activation energy, ΔE_A, and found $\Delta E_A = 56$ kJ mol^{-1} in the B_2 phase and $\Delta E_A = 84$ kJ mol^{-1} in the B_5 phase.

Structures of mesophases were determined by X-ray diffraction studies. The X-ray pattern recorded for compound **IId** at 120 °C exhibits a series of sharp, commensurate small angle reflections and a diffuse scattering maximum in the wide angle region (Fig. 7). Such a pattern is characteristic for a lamellar structure with the liquid-like molecular packing within the layers, so it confirms the identification of the smectic B_2 phase.

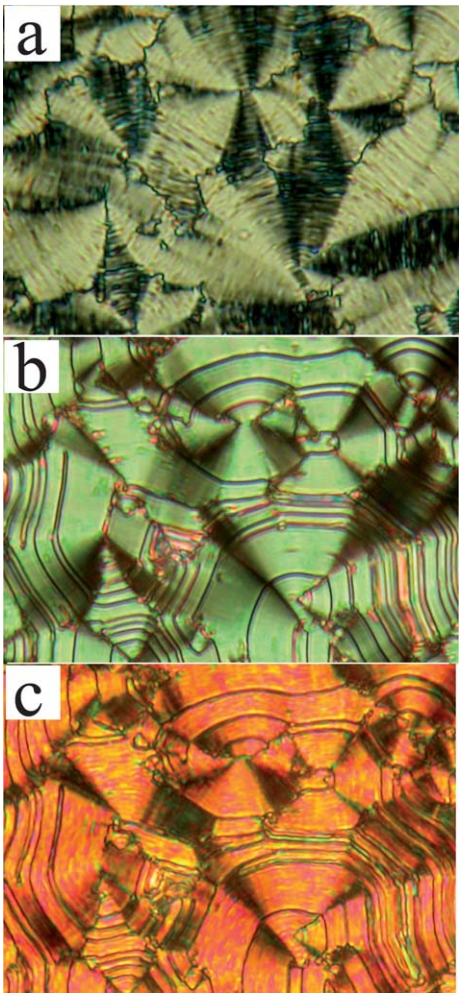

Fig. 4 Planar texture of compound **IId** in the SmC_AP_A phase (a) without electric field (after its application), under the electric field of about (b) 5 V μm^{-1} and (c) 10 V μm^{-1}. Crossed polarizers are parallel to the microphotograph edge. The width of the figure is about 150 μm.

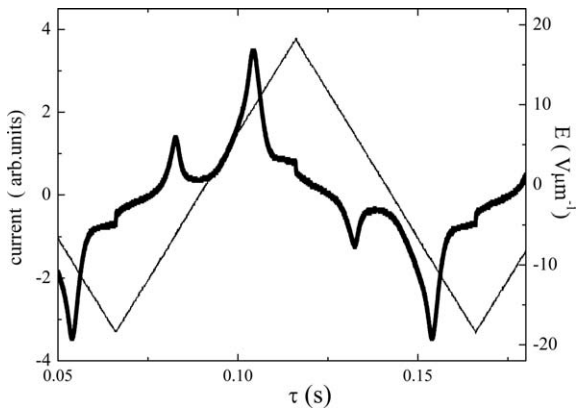

Fig. 3 Switching current profile for **IId** at a frequency of 10 Hz in the SmC_AP_A phase at $T = 110$ °C.

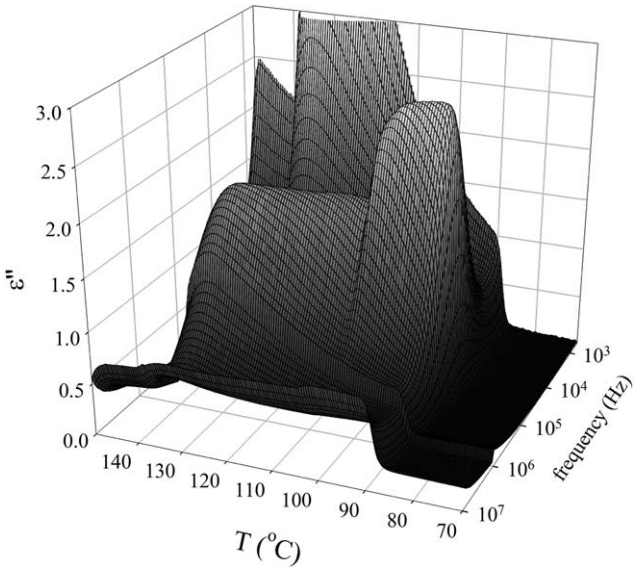

Fig. 5 3-Dimensional plot of the imaginary part of permittivity, ε'', *versus* temperature and frequency for **IId**.

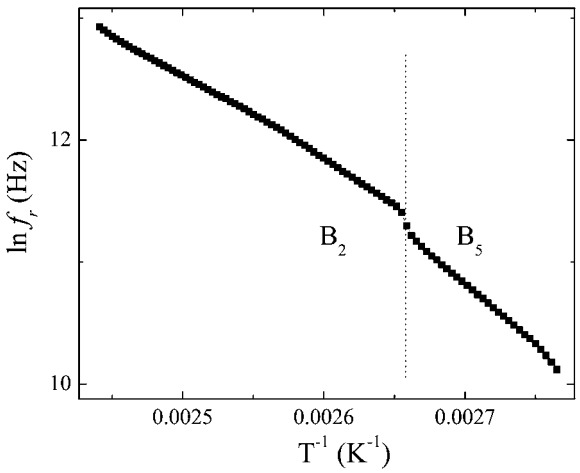

Fig. 6 The relaxation frequency, f_r, in a reciprocal temperature scale for **IId**.

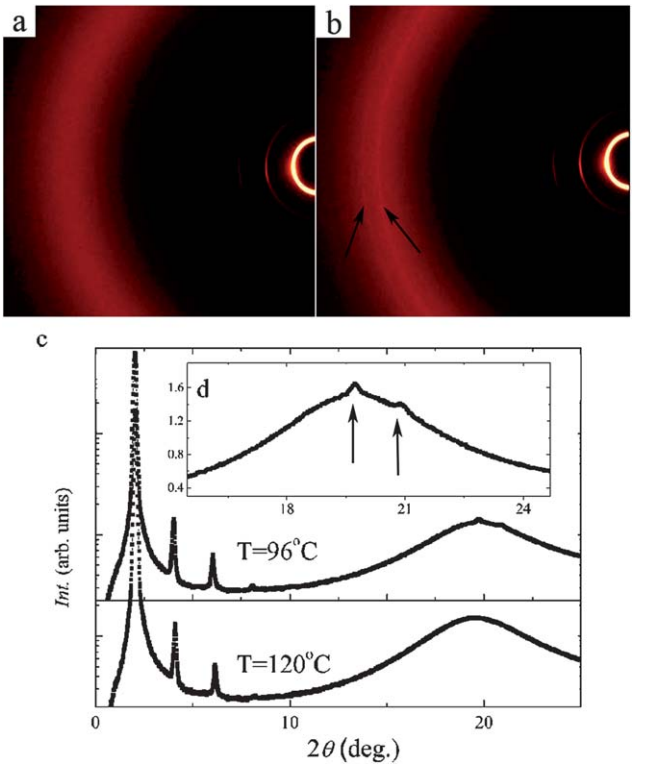

Fig. 7 2D X-ray patterns for the partially oriented sample of compound **IId** in (a) the B_2 phase at $T = 120$ °C and (b) the B_5 phase at $T = 96$ °C. (c) The intensity profile *versus* the scattering angle at $T = 120$ °C and $T = 96$ °C and (d) the wide angle range for $T = 96$ °C shown in an enlarged view (arrows mark sharp signals appearing in the B_5 phase).

The layer spacing, d, calculated from the position of the X-ray peaks, slightly increases on cooling (Fig. S3†). This effect can be caused by a gradual stretching of the terminal chains and/or increase of the orientational order of the molecules. By comparing the measured layer thickness with the estimated molecular length $l \approx 60$ to 61 Å, we can evaluate the tilt angle value, approximately 44–45 degrees, which is in agreement with the value determined from the rotation of extinction brushes in the fan-shaped texture of the sample exposed to electric field (see Fig. 4). At the B_2–B_5 phase transition all parameters of the X-ray pattern slightly change and, namely, the full-width at a half maximum, FWHM, exhibits a clear anomaly (Fig. S3†). The slope of the linear $d(T)$ dependence, which corresponds to the thermal expansion coefficient, α, changes at the B_2–B_5 phase transition; $\alpha = -0.02$ Å K^{-1} and -0.04 Å K^{-1} in the B_2 and B_5 phases, respectively. On the X-ray diffraction (XRD) pattern below the B_2–B_5 phase transition at $T = 100$ °C two additional sharp peaks appeared in the wide angle region, overlapped by the broad diffuse maxima (Fig. 7b and c). In the B_5 phase, the diffuse scattering remains and evidences still a high amount of disorder. Two additional maxima visible in the wide-angle range indicate a long-range in-plane positional correlation within the smectic layers. We observed two kinds of scattering in the B_5 phase: ordered in a two-dimensional lattice (the molecules from different layers are not correlated) and disordered centers, which give a broad diffuse halo. Such behavior is characteristic for the B_5 phase.[14]

Except for **IId**, all other compounds exhibited columnar phases with 2D periodic density modulations. Two types of the columnar phases were observed and distinguished by their XRD patterns. Low angle diffractograms for compounds **IIa–c** exhibited only two incommensurate sharp reflections (Fig. 8a) that can be indexed as (11) and (02) assuming centred rectangular unit cells. Such a pattern is typically attributed to the B_1 phase. XRD patterns registered for all compounds of series **I** and **III** were much richer (Fig. 8a), the signals could be indexed with a centred oblique unit cell; such diffractograms are typically ascribed to B_{1Rev} type phases. In all cases the crystallographic lattice parameters were weakly temperature dependent, the parameter related to layer fragment thickness grows on cooling, while the behaviour of the other unit cell dimension related to the molecular block size depends on the phase type,

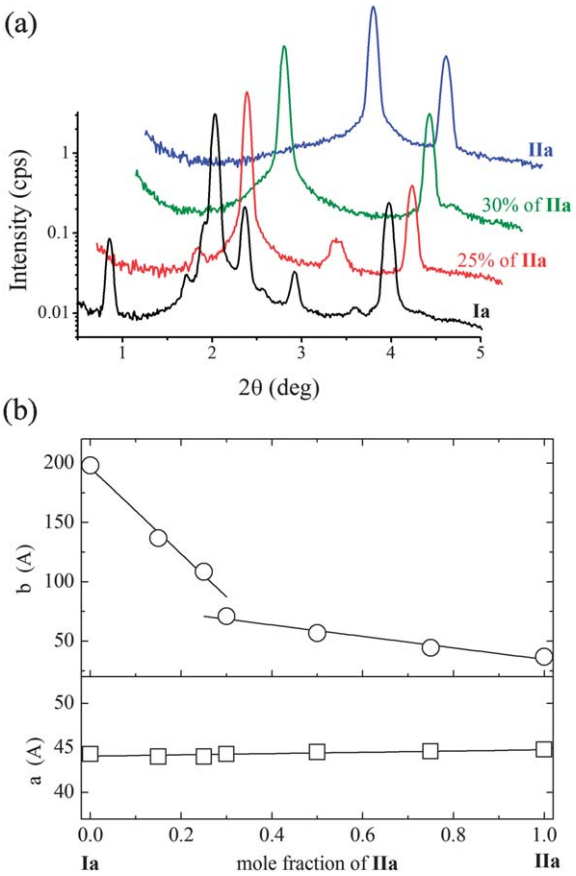

Fig. 8 (a) X-ray intensity *versus* the scattering angle for compounds **Ia** and **IIa** and their mixtures. (b) Evolution of the crystallographic unit cell parameters *a* and *b* with changing the composition of the mixtures of **Ia** and **IIa** compounds. Lines are guides for the eye.

in the B_1 phase (compounds of series **II**), the size of the column decreases on cooling, while in the B_{1Rev} phase (compounds of series **I** and **III**) the column size increases on cooling (Fig. S4†).

In order to check the phase identification, the miscibility experiments were conducted. Analogous compounds from series **I** and **II**, having the same length of the terminal chains, have been chosen, differing only in the orientation of one ester group in the mesogenic core. A very similar chemical structure of compounds **Ia** and **IIa** gives the opportunity to study mixtures with a very small two-phase region. The parameters of the crystallographic unit cell of the B_{1Rev} phase change continuously when component **IIa** is added to the **Ia** matrix (Fig. 8b), the cell inclination angle approaches 90 degree, the cross-section of the molecular blocks decreases and the intensity of signals (20) and (31) decreases. At the critical concentration, ~30% of compound **IIa**, the crystallographic unit cell for both phases B_1 and B_{1Rev} becomes identical, or nearly identical. However, the contact cell, prepared with two mixtures close to the critical concentration, still shows the phase boundary, the textures are different (Fig. 9). Based on this experiment, the question arises: what is the difference between these two phases? Both phases are made of smectic layer fragments being vertically shifted one against another. The lowering intensity of the (20) signal in the

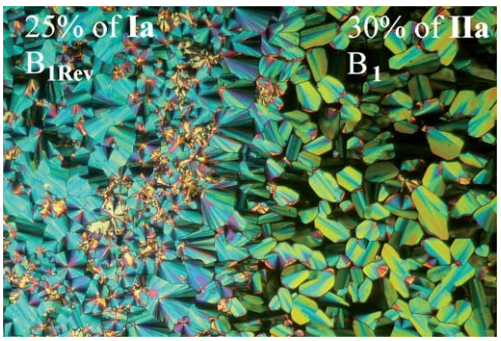

Fig. 9 Optical textures of the B_1 and B_{1Rev} phases taken for contact cell prepared with two mixtures of **Ia** and **IIa** compounds close to the critical concentration, a clear phase boundary is seen.

B_{1Rev} phase on approaching the critical concentration and the absence of this signal in the B_1 phase formed for mixtures above the critical concentration suggests that the phases differ in the defect separating neighbouring blocks. In the B_{1rev} phase the regions between blocks are filled with the molecules that strongly splay their polarization vectors[15d] and in the B_1 phase the blocks are attached to each other. Apparently, in the binary mixtures the width of the 'defect' region between the blocks decreases with the growing concentration of the **IIa** component.

4 Discussion and conclusions

Herein we report for the first time bent-shaped materials based on a 3-hydroxycinnamic acid central core. We have synthesized three series (denoted **I**, **II** and **III**) and modified the ester-group orientation and the length of the terminal alkyl chain. Regardless of the length of the terminal chain, the transition temperatures of compounds **I** are nearly identical. All compounds **I** exhibit the formation of the polar columnar B_{1Rev} phase. The same behaviour was observed for compounds **III** with five uniformly oriented ester groups. The presence of an additional ester group in the terminal chain caused only a slight decrease in the clearing temperatures, by 5–7 °C. The change of the orientation of the outer ester group in the lengthening arm in compounds **II** led to a decrease of both the melting and the clearing temperature. At the same time, the effect of the terminal chain length on mesomorphic properties is well documented for substances **II**. The temperature interval of the columnar mesophases dropped from the width of 80 °C for **IIa** to 52 °C for **IIc**. Finally, for compound **IId** with the longest terminal chain two lamellar phases (B_2 and B_5) appeared instead of the B_1 phase. The formation of lamellar phases for compounds with longer alkyl terminal chains has already been reported earlier for various bent-shaped mesogens.[13,16] The B_5 phase occurrence is rather unique,[11,14] because in smectic phases of bent-shaped mesogens a short range positional order in layers is usually observed.

When compared to the previously studied naphthalene based mesogens,[11,13] we can claim that the substitution of one of the benzene rings for a *trans*-double bond in studied materials **I–III** generally results in a decrease of the π–π interactions of

the aromatic rings. It leads to a lower rigidity of the central unit, thus to a decrease of the clearing temperatures of compounds **I–III**. The mesomorphic behaviour of compounds **I–III** is similar to that of the naphthalene based mesogens, where predominantly various columnar phases were detected, and only for the homologues with long terminal chains a lamellar B_2 phase appeared. It is also worth noting that some intermediates, silyl derivatives **3E–3H** and hydroxy derivatives **4E–4L**, exhibited the mesomorphic behaviour, and calamitic mesophases (nematic, SmA and SmC phases) were observed.

To summarize, the studied cinnamic acid-based bent-shaped materials with the uniform orientation of ester groups (series **I** and **III**) prefer the formation of the columnar phases of the B_{1Rev} type. For compounds **IIa–IIc** the B_1 phase has been detected. Both columnar mesophases, the B_{1Rev} and the B_1 phase, have been characterized by X-ray measurements. It has been demonstrated that the structural parameters of B_{1Rev} and B_1 phases can be continuously tuned when preparing binary mixtures of homologues **I** and **II**. For material **IId** with the tetradecyl terminal alkyl chain the presence of two polar lamellar switchable phases (B_2 and B_5) has been proved.

Acknowledgements

This work was supported by the Czech Science Foundation (projects P204/11/0723 and CSF 13-14133S).

References

1 (*a*) T. Niori, T. Sekine, J. Watanabe, T. Furukawa and H. Takezoe, *J. Mater. Chem.*, 1996, **6**, 1231–1233; (*b*) D. R. Link, G. Natale, R. Shao, J. E. Maclennan, N. A. Clark, E. Körblova and D. M. Walba, *Science*, 1997, **278**, 1924–1927.

2 G. Pelzl, S. Diele and W. Weissflog, *Adv. Mater.*, 1999, **11**, 707–724.

3 (*a*) W. Weissflog, H. Nádasi, U. Dunemann, G. Pelzl, S. Diele, A. Eremin and H. Kresse, *J. Mater. Chem.*, 2001, **11**, 2748–2758; (*b*) R. Amarantha Reddy and C. Tschierske, *J. Mater. Chem.*, 2006, **16**, 907–961; (*c*) H. Takezoe and Y. Takanishi, *Jpn. J. Appl. Phys.*, 2006, **45**, 597–625; (*d*) W. Weissflog, H. N. Shreenivasa Murthy, S. Diele and G. Pelzl, *Philos. Trans. R. Soc., A*, 2006, **364**, 2657–2679; (*e*) U. Dunemann, M. W. Schroeder, R. Amarantha Reddy, G. Pelzl, S. Diele and W. Weissflog, *J. Mater. Chem.*, 2005, **15**, 4051–4061.

4 J. Etxebarria and M. Blanca Ros, *J. Mater. Chem.*, 2008, **18**, 2919–2926.

5 N. Boiko, X. Zhu, A. Bobrovsky and V. Shibaev, *Chem. Mater.*, 2001, **13**, 1447–1452.

6 H. Kihara and N. Tamaoki, *Macromol. Rapid Commun.*, 2006, **27**, 829–834.

7 (*a*) I. C. Pintre, J. L. Serrano, M. Blanca Ros, J. Martinez-Perdiguero, I. Alonso, J. Ortega, C. L. Folcia, J. Etxebarria, R. Alicante and B. Villacampa, *J. Mater. Chem.*, 2010, **20**, 2965–2971; (*b*) H. Kihara and N. Tamaoki, *Liq. Cryst.*, 2007, **34**, 1337–1347.

8 (*a*) P.-C. Yang and J.-H. Liu, *J. Polym. Sci., Part A: Polym. Chem.*, 2008, **46**, 1289–1304; (*b*) A. Bobrovsky, V. Shibaev, V. Hamplová, M. Kašpar, V. Novotná, M. Glogarová and E. Pozhidaev, *Liq. Cryst.*, 2009, **36**, 989–997; (*c*) C. Keith, A. Lehmann, U. Baumeister, M. Prehm and C. Tschierske, *Soft Matter*, 2010, **6**, 1704–1721.

9 (*a*) R. Amarantha Reddy, B. K. Sadashiva and S. Dhara, *Chem. Commun.*, 2001, 1972–1973; (*b*) E. Mátyus and K. Fodor-Csorba, *Liq. Cryst.*, 2003, **30**, 445–450; (*c*) H. N. Shreenivasa Murthy and B. K. Sadashiva, *Liq. Cryst.*, 2004, **31**, 1347–1356; (*d*) R. Amarantha Reddy, B. K. Sadashiva and V. A. Raghunathan, *Chem. Mater.*, 2004, **16**, 4050–4062.

10 (*a*) R. Amarantha Reddy, B. K. Sadashiva and U. Baumeister, *J. Mater. Chem.*, 2005, **15**, 3303–3316; (*b*) W. Weissflog, U. Dunemann, S. Findeisen-Tandel, M. G. Tamba, H. Kresse, G. Pelzl, S. Diele, U. Baumeister, A. Erermin, S. Stern and R. Stannarius, *Soft Matter*, 2009, **5**, 1840–1847.

11 G. Pelzl, M. G. Tamba, S. Findeisen-Tandel, M. W. Schröder, U. Baumeister, S. Diele and W. Weissflog, *J. Mater. Chem.*, 2008, **18**, 3017–3031.

12 (*a*) W. Weissflog, G. Nauman, B. Košata, M. W. Schröder, A. Eremin, S. Diele, Z. Vakhovskaya, H. Kresse, R. Friedmann, S. A. R. Krishnan and G. Pelzl, *J. Mater. Chem.*, 2005, **15**, 4328–4337; (*b*) S. Ananda Rama Krishnan, W. Weissflog, G. Pelzl, S. Diele, H. Kresse, Z. Vakhovskaya and R. Friedemann, *Phys. Chem. Chem. Phys.*, 2006, **8**, 1170–1177.

13 (*a*) M. Kohout, J. Svoboda, V. Novotná, D. Pociecha, M. Glogarová and E. Gorecka, *J. Mater. Chem.*, 2009, **19**, 3153–3160; (*b*) M. Kohout, J. Svoboda, V. Novotná, M. Glogarová and D. Pociecha, *Liq. Cryst.*, 2010, **37**, 987–996; (*c*) M. Kohout, J. Svoboda, V. Novotná and D. Pociecha, *Liq. Cryst.*, 2011, **38**, 1099–1110.

14 (*a*) R. Amaranatha Reddy and C. Tschierske, *J. Mater. Chem.*, 2006, **16**, 907–961; (*b*) H. Nádasi, W. Weissflog, A. Eremin, G. Pelzl, S. Diele, B. Das and S. Grande, *J. Mater. Chem.*, 2002, **12**, 1316–1324.

15 (*a*) J. Szydlowska, J. Mieczkowski, J. Matraszek, D. W. Bruce, E. Gorecka, D. Pociecha and D. Guillon, *Phys. Rev. E: Stat., Nonlinear, Soft Matter Phys.*, 2003, **67**, 031702; (*b*) E. Gorecka, N. Vaupotić, D. Pociecha, M. Cepić and J. Mieczkowski, *ChemPhysChem.*, 2005, **6**, 1087–1093; (*c*) E. Gorecka, N. Vaupotic and D. Pociecha, *Chem. Mater.*, 2007, **19**, 3027–3031; (*d*) N. Vaupotic, M. Copic, E. Gorecka and D. Pociecha, *Phys. Rev. Lett.*, 2007, **98**, 247802.

16 (*a*) J. Svoboda, V. Novotná, V. Kozmik, M. Glogarová, W. Weissflog, S. Diele and G. Pelzl, *J. Mater. Chem.*, 2003, **13**, 2104–2110; (*b*) V. Kozmík, M. Kuchař, J. Svoboda, V. Novotná, M. Glogarová, U. Baumeister, S. Diele and G. Pelzl, *Liq. Cryst.*, 2005, **32**, 1151–1160; (*c*) V. Kozmík, A. Kovářová, M. Kuchař, J. Svoboda, V. Novotná, M. Glogarová and J. Kroupa, *Liq. Cryst.*, 2006, **33**, 41–56; (*d*) V. Kozmík, P. Polášek, A. Seidler, M. Kohout, J. Svoboda, V. Novotná, M. Glogarová and D. Pociecha, *J. Mater. Chem.*, 2010, **20**, 7430–7435.